Wei, Tzu-Chiao, Mokkapati, Sudha , Li, Ting-You, Lin, Chun-Ho, Lin, Gong-Ru, Jagadish, Chennupati and He, Jr-Hau 2018. Nonlinear absorption applications of $CH_3NH_3PbBr_3$ perovskite crystals. Advanced Functional Materials 10.1002/adfm.201707175

Publishers page: https://doi.org/10.1002/adfm.201707175

ToC

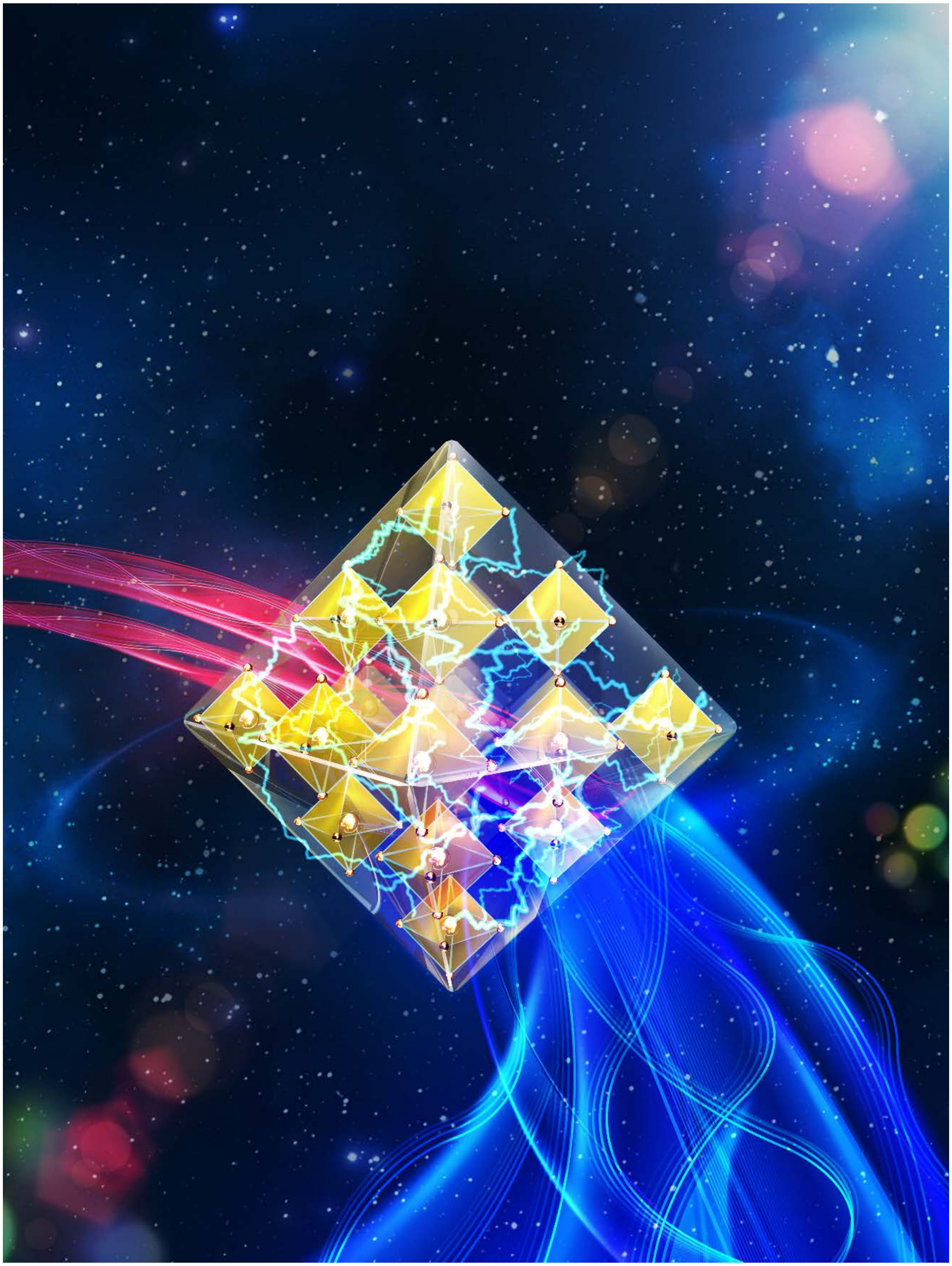

Nonlinear Absorption Applications of $CH_3NH_3PbBr_3$ Perovskite Crystals

Tzu-Chiao Wei,[1,2] Sudha Mokkapati,[4] Ting-You Li,[1] Chun-Ho Lin,[1] Gong-Ru Lin,[3]
Chennupati Jagadish,[2] and Jr-Hau He[1,*]

[1]Computer, Electrical, and Mathematical Sciences and Engineering Division, King Abdullah University of Science & Technology, Thuwal 23955-6900, Saudi Arabia

[2]Department of Electronic Materials Engineering, Research School of Physics and Engineering, Australian National University, Canberra, A.C.T. 2601, Australia

[3]Institute of Photonics and Optoelectronics, National Taiwan University, Taipei 10617, Taiwan

4School of Physics and Astronomy, North Queens Building, The Parade, Cardiff University, Cardiff, UK – CF24 3AA

[*]jrhau.he@kaust.edu.sa; Chennupati.Jagadish@anu.edu.au

Abstract

Researchers have recently revealed that hybrid lead halide perovskites exhibit ferroelectricity, which is often associated with other physical characteristics, such as a large nonlinear optical response. In this work, we study the non-linear optical properties of single crystal inorganic-organic hybrid perovskite $CH_3NH_3PbBr_3$. By exciting the material with a 1044 nm laser, we were able to observe strong two-photon absorption-induced photoluminescence in the green spectral region. Using the transmission open-aperture Z-scan technique, we estimated the values of the two-photon absorption coefficient to be 8.5 cm GW^{-1}, which is much higher than that of standard two-photon absorbing materials that are industrially used in nonlinear optical applications, such as $LiNbO_3$, $LiTaO_3$, $KTiOPO_4$, and KH_2PO_4. Such a strong two-photon absorption effect in $CH_3NH_3PbBr_3$ can be used to modulate the spectral and spatial profiles of laser pulses, as well as reduce noise, and can be used to strongly control the intensity of incident light. In this study, we demonstrate the superior optical limiting, pulse reshaping, and stabilization properties of $CH_3NH_3PbBr_3$, opening new applications for perovskites in nonlinear optics.

Keywords: perovskite, $CH_3NH_3PbBr_3$, two-photon absorption, nonlinear optics, optical limiting, pulse reshaping, optical stabilization

Two-photon absorption (TPA) is a third-order nonlinear optical process involving two coherent photons that promote an electron to an excited state, the gap of which corresponds to the combined energies of both photons. Nonlinear optical materials play a major role in the field of photonics and are expected to become key materials for emerging technologies, such as optical information and communication processing,[1,2] sensor protection applications, and more.[3,4] In recent decades, ammonium dihydrogen phosphate and potassium dihydrogen phosphate have been the premier nonlinear optical crystals for TPA-related applications, in part because they can be grown at large scale. Lithium niobate ($LiNbO_3$) has also emerged as a promising TPA material based on its high optical nonlinearity coefficient, which is ten-times larger than that of ammonium and potassium dihydrogen phosphate.[5] However, the relatively low optical damage threshold of these materials limits their practicality in operations that require high-intensity laser irradiation.[6] In the search for more robust TPA compounds, one strategy is look to materials that demonstrate ferroelectric properties, which due to large spontaneous polarization and high dielectric constants tend to also display a large nonlinear optical response.[7–9]

Researchers recently confirmed the ferroelectric domain of hybrid lead halide perovskites,[10,11] a property which appears related to the presence of polar molecular cations in the crystalline framework.[12] These ferroelectric domains may aid the separation of photoexcited electron-hole pairs and reduce charge carrier recombination.[13] Hence, it can be expected that hybrid lead halide perovskites exhibit high optical nonlinearity,[14] a hypothesis which was recently confirmed.[15,16]

Perovskites have already shown exciting promise in applications of photovoltaics,[17–19] light emitting diodes,[20–22] and other optoelectronic devices,[23] and as a result have attracted increased research focus over recent years. Using an inexpensive and room-temperature process,[19] researchers have been able to easily synthesize these materials and demonstrate their unique electronic and linear optical properties, establishing perovskites as a new class of semiconductors. Following the discovery of these unique properties has been the development of new optoelectronic applications, including lasers,[24] data storage,[25] and optomechanical sensors.[26,27] However, neither the physical mechanisms nor the theoretical models of the nonlinear phenomena in perovskites have been studied in detail for optical applications.

In this study, we measure TPA-induced photoluminescence (PL) in single crystal methylammonium lead bromide ($CH_3NH_3PbBr_3$ or $MAPbBr_3$) as well as the corresponding TPA coefficient using the transmission open-aperture Z-scan technique at an excitation wavelength of 1044 nm. With this method we were able to study the physical mechanism of optical nonlinearity in $MAPbBr_3$ and demonstrate several TPA-based nonlinear optical applications, including optical limiting, stabilization, and reshaping of laser pulse signals. These properties are essential for practical applications in any optical system and can be used to control laser noise, modulate various electromagnetic fields, and protect delicate optical sensors. These theoretical and experimental advances in $MAPbBr_3$ nonlinear optical applications suggest new potential for perovskite photonics.

Results and discussion

The anti-solvent vapor-assisted crystallization method was used to grow large single crystal $MAPbBr_3$ perovskite for nonlinear optical characterization. The $MAPbBr_3$ crystal

(2.8 mm in length, 2.7 mm in width, and 3.8 mm in thickness) appeared orange-colored and featured rectangular facets, as shown in Figure 1a.

We determined our synthesized material featured a perovskite phase using powder X-ray diffraction (XRD). As shown in Figure 1b, the diffraction peaks at 15.16º, 21.37º, and 30.3º corresponding to the (001), (011), and (002) lattice planes of the cubic structure, respectively, are consistent with previously reported single crystal $MAPbBr_3$ grown at room temperature.[28–30] The XRD pattern also shows that the $MAPbBr_3$ sample has a highly crystalline cubic phase. The XRD analysis reveals the material is also single crystal (see Table S1 for more details).[28] Figure 1c shows the unit cell of $MAPbBr_3$. The material adopts the bonding structure typical of perovskites, which can be described by the chemical formula ABX_3, where A and B represent cations of different sizes and X is an anion that bonds to both A and B. In $MAPbBr_3$, the organic cation A is methylammonium ($CH_3NH_3^+$), the metal cation B is Pb^{2+}, and the anion X is the halogen Br^{1-}. The methylammonium cation is surrounded by $PbBr_6$ octahedra.

To understand the thermal properties of the single crystal $MAPbBr_3$, we performed thermogravimetric analysis (TGA; Figure 1d). The thermal decomposition of $MAPbBr_3$ began and finished at temperatures of 320 °C and 592.1 °C, respectively. The material exhibits a two-step decomposition process with weight losses of 23.4% and 14.2% at each step. Note that materials used for optical devices must exhibit high thermal stability in order to avoid significant distortion caused by illumination-induced thermal gradients and damage.[31,32] As compared with many polymers and organic TPA materials, the thermodynamic stability of $MAPbBr_3$ is relatively high. In contrast, the related perovskite $CH_3NH_3PbI_3$ begins to decompose at a temperature of 294 °C.[33,34] Additionally, $MAPbBr_3$

is known to be more stable in air.[31] The enhanced ambient and thermal stability of $MAPbBr_3$ can be attributed to its cubic structure and strong Pb−Br bonds.[32] The advantages of this material thus motivated us to study its TPA and related applications.

Two-photon excited fluorescence and a simplified energy-level diagram of the TPA process are shown in Figure 2a. The mechanism is initiated by the simultaneous absorption of two photons featuring energies of less than the absorbing material’s bandgap. Subsequent fluorescence occurs through the emission of a single photon at a higher energy. We can observe this process with the naked eye, as shown on the right-hand side of Figure 2a, in which the $MAPbBr_3$ crystal displays green fluorescence as it is pumped with a pulsed laser at a lower energy wavelength of 1044 nm and power density of 0.1 MW cm^{-2}. Figure 2b shows the linearly and nonlinearly (*i.e.*, TPA) photoexcited PL spectra of the $MAPbBr_3$, excited with 522 nm and 1044 nm wavelengths, respectively. The TPA-induced emission occurs at 550 nm with a full width at half maximum of 17 nm. The same green emission can be seen while exciting the $MAPbBr_3$ sample with the 522 nm laser *via* linear single-photon absorption.[37] The linear and nonlinear PL spectra line shapes are slightly asymmetric, which can be decomposed into the contribution of states from residual $PbBr_2$.[38] This is also supported by evidence of a small XRD signal at $2\theta = 16^{\circ} \sim 17^{\circ}$ next to the (001)-oriented $MAPbBr_3$-related XRD peak at 15.16°.[39] These $PbBr_2$ composites are known to assist the radiative process in $MAPbBr_3$.

In principle, the nonlinear optical properties of a medium can be expressed using the high-order terms in a Taylor series expansion of the dielectric polarization density as a function of the applied electric field (E).[40] The dielectric polarization density (P) is given as:

$$P_i = \varepsilon_0\left(\mathcal{X}_{ij}^{(1)}E_j + \mathcal{X}_{ijk}^{(2)}E_jE_k + \mathcal{X}_{ijkl}^{(3)}E_jE_kE_l + \cdots\right), \qquad (1)$$

in which χ is the n^{th}-order susceptibility of the medium. The first term on the right-hand side of the equation represents the linear response of the medium when the dielectric polarization is the same frequency as the applied electric field. The second and third terms represent the second- and third-order optical nonlinearities, which involve at least two applied electric fields that can induce a new polarization field at a different frequency.

To confirm the applicability of Equation (1), we characterized the polarization dependence of the perovskite's TPA, as it strongly depends on the crystal symmetry (Figure 2c).[41] The polarization dependent emission spectra were measured using a normal-incidence backscattering geometry as the laser polarization was rotated around the perpendicular axis of the $MAPbBr_3$ crystal orientation (see inset of Figure 2d). According to the selection rule of second-harmonic generation, PL intensity measured at the normal backscattering geometry should follow:[42]

$$S = \eta \times \sin^2(2\theta)\ , \qquad (2)$$

in which S is the PL intensity, η is a proportionality constant, and Θ is the rotation angle of the linear polarizer. As shown in Figure 2d, when we plotted the emission intensity of the $MAPbBr_3$ as a function of the rotation angle Θ, the result demonstrated 90° periodicity with maxima at $\Theta = 45°$, and 135°, in agreement with the fitted $\sin^2(2\Theta)$ dependence described in Equation (2). Such a four-fold symmetry of the polarization angle-dependent PL certifies that the perovskite lattice exhibits a four-fold rotational symmetry along the *c*-axis.[41,43,44] This is also strong evidence confirming the single crystallinity of the $MAPbBr_3$ sample as the four-fold symmetry of the polarization angle dependent PL cannot be observed in polycrystalline materials.[45]

In Figure 2e, we demonstrate the power dependence of the TPA-induced PL of the single crystal $MAPbBr_3$ at room temperature by increasing the pumping power (*i.e.*, intensity) of the 1044 nm exciting laser from 0.58 mW (0.001 MW cm^{-2}) to 2.57 mW (0.004 MW cm^{-2}). The resulting PL emission intensity at 550 nm as a function of the excitation power can be fit with a quadratic relation (Figure 2f), revealing that the PL of the single crystal $MAPbBr_3$ is mainly due to the TPA process.[46,47]

To quantify the optical nonlinearity of the $MAPbBr_3$, we employed the transmission open-aperture Z-scan technique, which is a highly sensitive single-beam experimental method for determining TPA coefficients.[48] The Z-scan technique is described in detail in Ref. 48. A standard Z-scan analysis is done by moving the sample back-and-forth from the focal point of the pulsed laser beam along its optical axis (defined as the z-axis) *via* a continuously tunable optical attenuator plate. Under the assumption that the laser beam intensity follows an ideal Gaussian profile, the normalized open-aperture Z-scan transmittance can be given by:[49]

$$T_{TPA} = \left[1 + (n-1)\alpha_n L_{eff}\left(I_0/(1+(z/z_0)^2)\right)^{n-1}\right]^{-1/(n-1)}$$

$$L_{eff} = \frac{1-e^{-\alpha L}}{\alpha} \qquad (3)$$

in which α_n denotes the effective multiphoton absorption coefficient, L_{eff} is the effective length of the sample, α is the linear absorption coefficient, L is the actual length of the sample, I_0 is the laser intensity, and z_0 is the diffraction length of the laser beam (also known as the Rayleigh length). Using Equation 3 to fit the Z-scan experimental data shown in Figure 3, we numerically calculated the effective TPA coefficient (α_2) as 8.5 cm GW^{-1} for the single crystal $MAPbBr_3$ at 1044 nm excitation, which is significantly higher than other well-known semiconductors that feature TPA at similar wavelengths, such as CdTe (0.02

cm GW^{-1} at 1300 nm)[50] and GaSe (～6.3 cm GW^{-1} at 1060 nm).[51] The TPA coefficient of $MAPbBr_3$ is much higher than other commonly used TPA crystals, such as $LiNbO_3$ (3.5 cm GW^{-1} at 388 nm),[52] $LiTaO_3$ (2 cm GW^{-1} at 800 nm),[53] $KTiOPO_4$ (1.8 cm GW^{-1} at 800 nm),[54] and KH_2PO_4 (0.3 cm GW^{-1} at 532 nm).[55] It is also 17-times greater than that of single crystalline Si (～0.5 cm GW^{-1} at near-infrared wavelengths).[56–58]

Such a strong TPA effect observed in single crystal $MAPbBr_3$ opens it to potential applications in optical switching and limiting devices, which require large optical nonlinearity.[59,60] For example, when an optical signal passes through such a medium, large TPA can help to nonlinearly scale down the transmission of the optical wave. In this manner, any intensity fluctuation of the incident light can be significantly suppressed to provide a more stabilized output. To study the optical stabilization properties of $MAPbBr_3$, we compared the signal intensity fluctuations of both the optical input and output laser pulses in Figure 4a,b. The relative intensity noise can be given by the following equation:

$$\frac{S_{max}-S_{min}}{(S_{max}+S_{min})/2}\times 100\% \tag{4}$$

in which S_{max} and S_{min} are the strongest and lowest signal intensity, respectively. As expected, the laser beam with a relative intensity noise of approximately ± 2.4% at the input signal can be effectively reduced to about ± 0.34% for the output pulse, indicating that nearly one-order-of-magnitude reduction of the fluctuation in noise can be achieved by utilizing the TPA properties of single crystal $MAPbBr_3$ for superior optical stabilization. For comparison, epoxy rod and neat liquid crystal can only stabilize the optical power fluctuations of the laser by a factor of 2.8 and 2.2, respectively.[61,62] These results demonstrate that $MAPbBr_3$ is capable of performing the optical stabilization needed to reduce the relative intensity fluctuation of lasers (*i.e.*, noise) and can be applied to a laser system as an optical power stabilizer.[62,63]

Controlling the amplitude, phase, and frequency modulation of electromagnetic fields has proven useful for a wide range of applications in spectroscopy.[64] Materials that feature large TPA can also play important roles in reshaping the spectral and spatial profiles of laser pulses.[65,66] Figure 4c shows the relative intensity of the spatial profile of the laser pulse. After passing through the $MAPbBr_3$ crystal, the profile of the output signal becomes much flatter and smoother (Figure 4d). The modulation depth (*i.e.*, the spatial intensity fluctuation, defined as the deviation of the peak amplitude over the mean of the amplitude) for the incident and transmitted laser pulses were estimated to be ～80% and ～35%, respectively. This reduction of the modulation depth of the optical wave after transmitting through single crystal $MAPbBr_3$ is 1.6-times greater than when an organic chromophore is used, such as AF-350, which researchers observed can reduce the modulation depth from ～67% to just ～39%.[65] The response time of this optical stabilization effect can almost be ignored, as the time delay between the input and output laser pulses is in the range of a few nanoseconds of the TPA-induced florescence. That is to say that the strong reshaping effect of $MAPbBr_3$ can be used to control the noise in the laser beam, which provides an attractive route for future optical-based modulators and optical communications based on spectral manipulation.

Due to its large TPA coefficient, it is expected that $MAPbBr_3$ can also serve as an effective optical limiter for laser pulses. An optical limiter is a device that strongly decreases the intensity of intense optical signals while maintaining relatively high transmittance for weak optical inputs.[67] Figure 4e shows the nonlinear output intensity versus the input intensity of a 300 fs laser pulse at a wavelength of 1044 nm and a repetition rate of 20.8 MHz. We observed that when this beam was placed through the $MAPbBr_3$ crystal, the transmittance increased from 0.38 W μm^{-2} to 1.03 W μm^{-2} as the input intensity increased from 0.61 W μm^{-2} to 4.97 W μm^{-2}, demonstrating the excellent optical limiting behavior of the perovskite. At low intensity, the laser passing through the $MAPbBr_3$ suffers from small loss of incident energy. Increasing the input laser intensity attenuates the transmitted signal, demonstrating a gradually saturating behavior of the transmitted laser pulse intensity. Such optical limiting behavior of a TPA medium at a fixed wavelength can be calculating using the following equation:[59]

$$I(x, L) = I(x, 0)T = \frac{\ln(1+\beta(\lambda)I(x,0)L)}{\beta(\lambda)L}, \tag{5}$$

in which $I(x,0)$ is the transverse intensity function of the optical incidence at wavelength λ, and β and L are the TPA coefficient and optical path length of the TPA medium, respectively. The calculated and measured results in Figure 4e correspond well when we applied the effective TPA coefficient that had been calculated from the numerical fitting in Figure 3 (α_2 = 8.5 cm GW^{-1}). This result strongly supports the validity of the TPA coefficient that we determined *via* the open-aperture Z-scan experiment.

Note that the optical limiting behavior is very sensitive to the size of the aperture in front of the detection unit, which can significantly block the output pulse's energy as it is being measured.[68] A larger aperture can be used to reduce the influence of other nonlinear processes, such as self-focusing, self-defocusing, and thermal effects occurring in nonlinearly absorbing media.[69] Figure 4f shows the nonlinear output energy versus the input energy of the laser pulse measured with an F/32 aperture located behind the medium but before the sensor. As a result, the nonlinear transmittance greatly decreases to 462 W μm^{-2} as the input intensity is increased from 606 W μm^{-2} to 4970 W μm^{-2}. This design improves the optical limiting performance of the perovskite simply by using an aperture in front of the detection unit. For future applications, single crystal $MAPbBr_3$ could be considered for the protection of delicate optical sensors, such as the human eye and charge-coupled device (CCD) detectors from high intensity laser radiation that could otherwise cause irreversible damage.

Conclusion

In summary, we investigated the TPA properties and demonstrated corresponding applications of inorganic-organic hybrid perovskite $MAPbBr_3$ crystals. The intense TPA-induced PL can be observed with a 1044 nm laser to pump the crystal. Using the transmission open-aperture Z-scan technique and theoretical fitting, we obtained an effective TPA coefficient for the material of 8.5 cm GW^{-1}. Moreover, we have demonstrated several nonlinear optical applications of the perovskite, including optical reshaping, stabilization, and limiting behavior on intense pulsed laser signals. Based on these results, we believe the organometallic trihalide perovskite holds great promise as a high-performance, low-cost nonlinear absorber for applications in ultrafast photonics.

Methods

Chemicals and reagents. Lead (II) bromide ($PbBr_2$, ≥98%), methylamine (CH_3NH_2, 40% wt/wt aqueous solution), N, N-dimethylformamide (DMF, ≥99.8%), dichloromethane (DCM, ≥99.8%), hydrobromic acid (HBr, 48% wt/wt aqueous solution, ≥99.99%) and ethanol (≥99.8%) were purchased from Sigma-Aldrich and used without further purification.

$MAPbBr_3$ single crystal synthesis. We first synthesized methylammonium bromide (CH_3NH_3Br) by stirring an equimolar solution of HBr and methylamine for 2 h at 10 °C, followed by recrystallization from ethanol. $MAPbBr_3$ crystals were then grown using the anti-solvent vapor-assisted crystallization method,[70] in which an equimolar amount of lead bromide ($PbBr_2$) and the CH_3NH_3Br crystals were dissolved in DMF, followed by the addition of DCM. The slow diffusion of DCM vapor through the solution helped initiate single crystal $MAPbBr_3$ growth.

X-ray diffraction. A small flake (~0.1 mm × 0.1 mm × 0.08 mm) was cleaved from the as-grown $MAPbBr_3$ crystal. We measured the XRD spectrum on a Bruker KAPPA APEX DUO Diffractometer using IμS Cu radiation at 296 K (λ = 0.71073 Å), and an APEX II 4K CCD detector. The phase purity was measured *via* powder XRD using a Bruker D8 Advance diffractometer (Bragg–Brentano geometry) equipped with a Cu Ka X-ray tube.

Thermogravimetric analysis. Thermoanalysis of the single crystal $MAPbBr_3$ sample was performed at a heating rate of 1 ºC min^{-1}, from 25 ºC up to 600 ºC under nitrogen atmosphere (99.999%, 20 ml/min) using a TGA combined with a mass spectrometer (NETZSCH TGA/STA-QMS 403 C).

Measurements of nonlinear optical properties. To study the nonlinear optical properties of $MAPbBr_3$, a frequency-doubled solid-state laser (femtoTRAIN IC-Yb-2000) was used to pump the perovskite crystal (λ_{pump} = 1044 nm, repetition rate = 20.8 MHz, pulse length = 300 fs) with a spot-size of ~8.5 μm in diameter. The $MAPbBr_3$ sample was excited through an aberration corrected 60×/0.70 numerical aperture and a long working distance objective lens (Nikon CFI Plan Fluor). The resulting emission was collected through the same objective, in which the incident and reflected light propagate parallel to the z-axis of the $MAPbBr_3$ crystal. The collected light was spectrally filtered to remove the pump laser wavelength. Spectral measurements were made using a grating spectrometer (Acton, SpectraPro 2750) featuring a resolution of 0.18 nm and a CCD detector (Princeton Instruments, PIXIS). For polarization analysis, a linear polarizer was inserted in the parallel beam path and the polarization axis was rotated to match the orientation of the crystal.

Acknowledgements

This work was financially supported by the King Abdullah University of Science and Technology (KAUST) Office of Sponsored Research (OSR-2016-CRG5-3005), KAUST solar center (FCC/1/3079-08-01), and KAUST baseline funding.

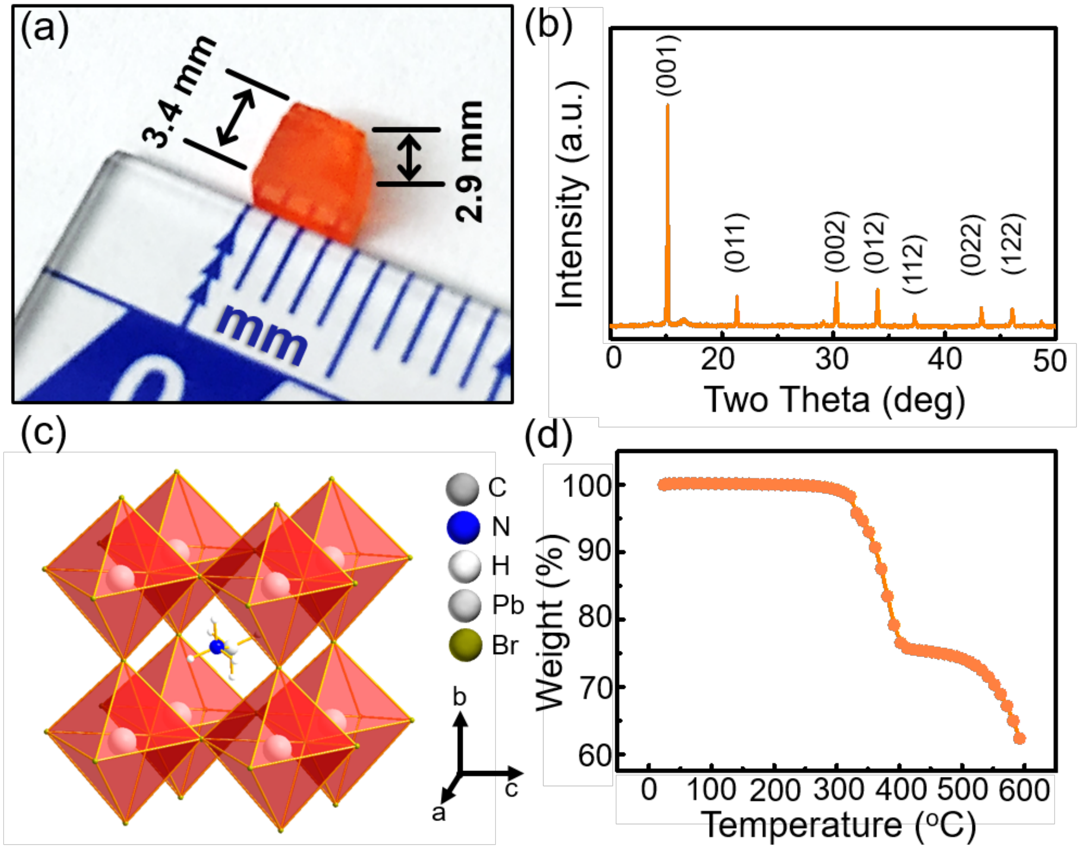

Figure 1. (a) An $MAPbBr_3$ single crystal grown by the anti-solvent vapor-assisted crystallization method. The size of this particular crystal was 3.8 x 3.4 x 2.9 mm. (b) The XRD spectrum of the $MAPbBr_3$ powder. (c) The crystal structure of the $MAPbBr_3$ perovskite as visualized through single crystal XRD. (d) The thermogram of single crystal $MAPbBr_3$ in Nitrogen atmosphere, displaying a two-step thermal decomposition process.

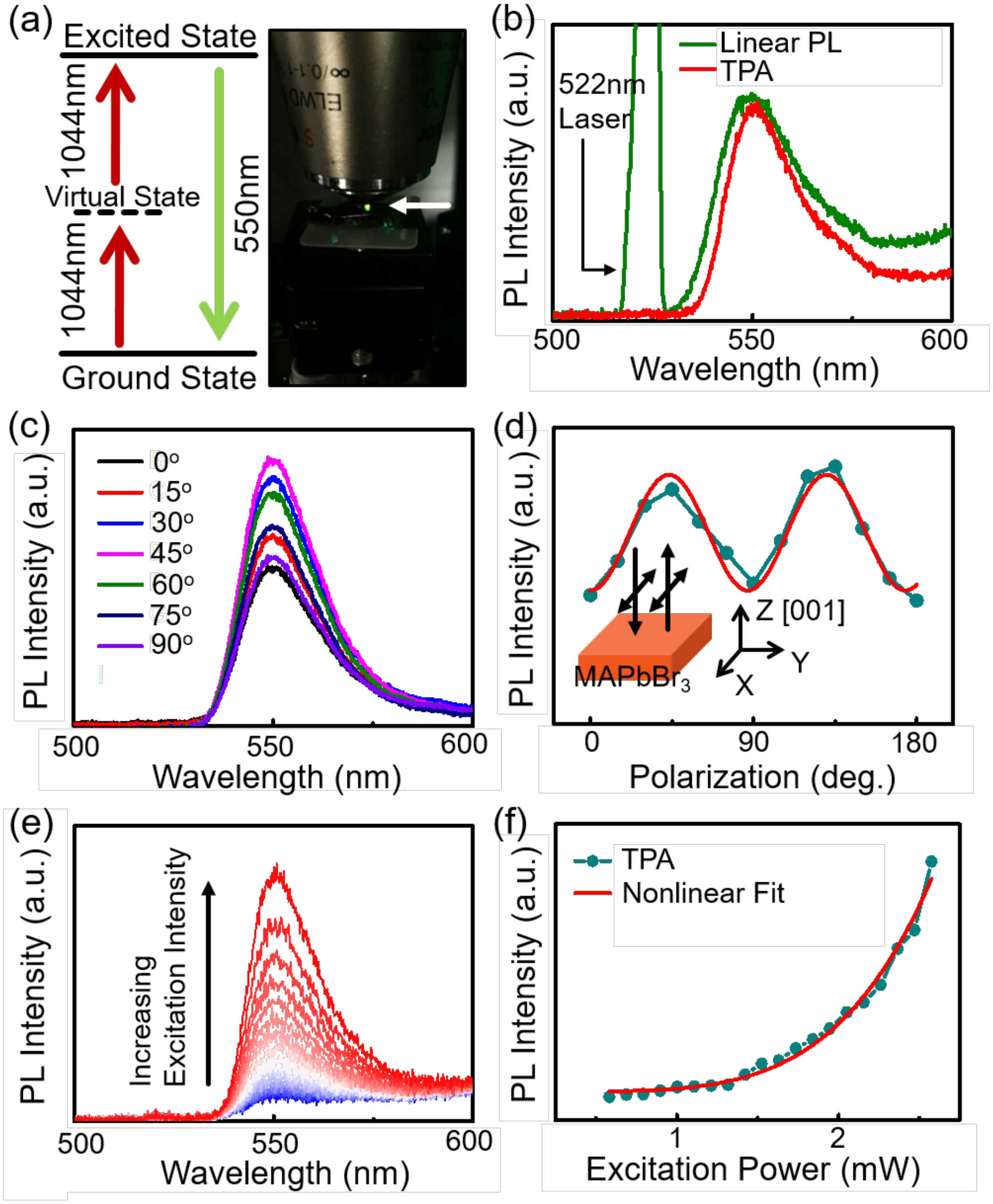

Figure 2. (a) A schematic of the TPA mechanism for the absorption of light at 1044 nm *via* two-photons and the resulting single-photon PL emission at 550 nm. The real eigenstates and intermediate state are represented by solid and dashed lines, respectively. The $MAPbBr_3$ fluorescence appears as the emission of green light (indicated by the arrow) that is visible to the naked eye. (b) The linear (green) and two-photon-induced (red) PL spectra

of $MAPbBr_3$ excited by 522 nm and 1044 nm laser wavelengths, respectively. (c) The polarization dependence of the two-photon-induced PL spectra of the $MAPbBr_3$ single crystal recorded at a rotation angle (Θ) from 0º to 90º measured in a backscattering geometry. (d) The rotation angle Θ *vs*. the intensity of the two-photon-induced PL emission at 550 nm. The solid line represents the best fit to the calculated polarization dependence of the PL using Equation (2). The inset shows the normal backscattering geometry used in the PL system. (e) The excitation power dependent two photon-induced PL spectra of $MAPbBr_3$. The black vertical arrow indicates the increasing excitation intensity, from 0.58 mW to 2.57 mW. (f) The evolution of the two-photon-induced PL intensity at 550 nm *vs*. the excitation power intensity.

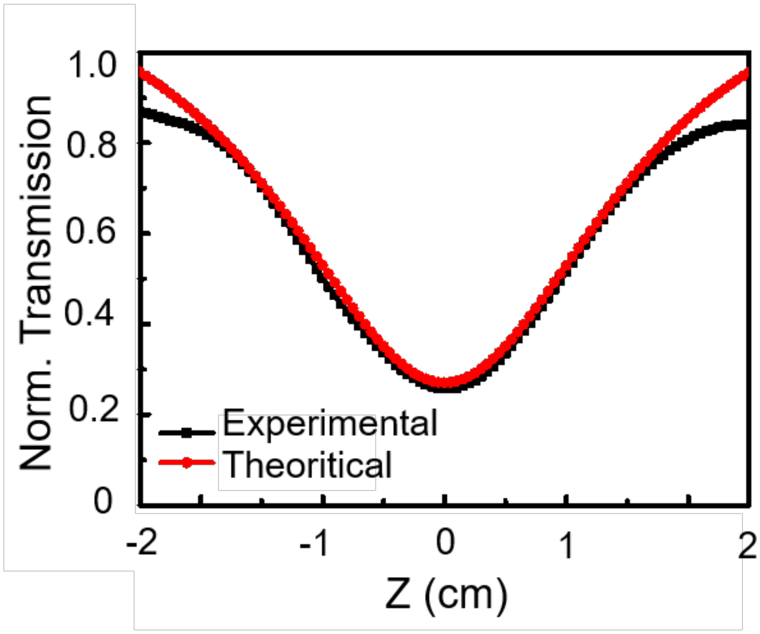

Figure 3. Open aperture Z-scan measurements (black) of the single crystal $MAPbBr_3$. An effective TPA coefficient of 8.5 cm GW^{-1} was obtained from the theoretical fitting (red) based on Equation (3).

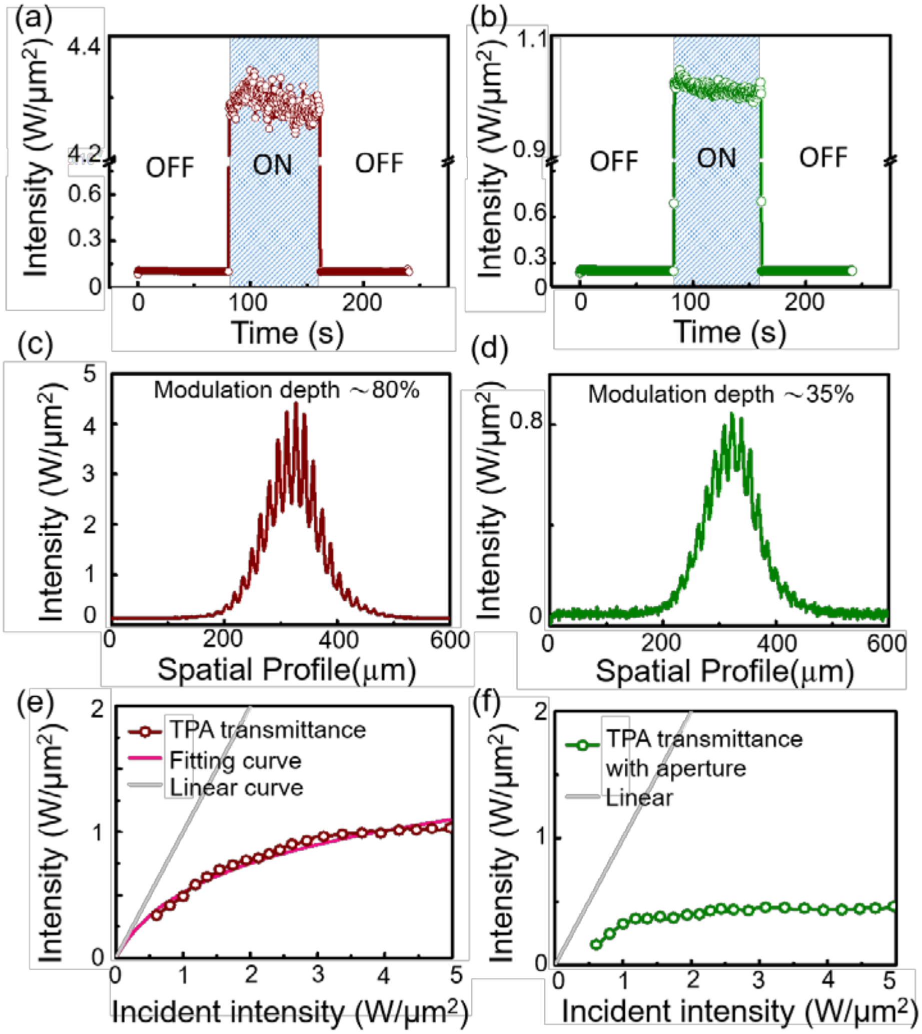

Figure 4. Intensity profiles of the (a) input and (b) output laser pulse fluctuations. The 1044 nm, 300 fs laser pulses at a 20.8 MHz repetition rate passed through the single crystal $MAPbBr_3$ sample. The relative pulse intensity distributions of the (c) input pulse and the (d) output pulse as it passed through the perovskite. (e) Optical limiting response of $MAPbBr_3$. The red best fitting curve incorporates an effective TPA coefficient of 8.5 cm GW^{-1}. (f) Measurement of the optical limiting effects of the $MAPbBr_3$ sample, using an experimental setup that featured an F/32 aperture before the detector.

Reference

(1) Cotter, D. Nonlinear Optics for High-Speed Digital Information Processing. *Science* **1999**, *286*, 1523–1528.

(2) Leuthold, J.; Koos, C.; Freude, W. Nonlinear Silicon Photonics. *Nat Phot.* **2010**, *4*, 535–544.

(3) Ganeev, R. A. *Nonlinear Optical Properties of Materials*; Springer Series in Optical Sciences; Springer Netherlands, 2013.

(4) Suresh, S.; Ramanand, A.; Jayaraman, D.; Mani, P. Review on Theoretical Aspect of Nonlinear Optics. *Reviews on Advanced Materials Science*, **2012**, *30*, 175–183.

(5) Boyd, G. D.; Miller, R. C.; Nassau, K.; Bond, W. L.; and Savage, A. $LiNbO_3$: AN EFFICIENT PHASE MATCHABLE NONLINEAR OPTICAL MATERIAL. *Appl. Phys. Lett.* **1964**, *5*, 234–236.

(6) Nakamura, M.; Higuchi, S.; Takekawa, S.; Terabe, K.; Furukawa, Y.; Kitamura, K. Optical Damage Resistance and Refractive Indices in near-Stoichiometric MgO-Doped $LiNbO_3$. *Japanese J. Appl. Physics, Part 2 Lett.* **2002**, *41*.

(7) Gu, B.; Wang, Y. H.; Peng, X. C.; Ding, J. P.; He, J. L.; Wang, H. T. Giant Optical Nonlinearity of a Bi2Nd2Ti3O12 Ferroelectric Thin Film. *Appl. Phys. Lett.* **2004**, *85*, 3687–3689.

(8) Shin, H.; Chang, H. J.; Boyd, R. W.; Choi, M. R.; Jo, W. Large Nonlinear Optical Response of Polycrystalline $Bi_{3.25}La_{0.75}Ti_3O_{12}$ Ferroelectric Thin Films on Quartz Substrates. *Opt. Lett.* **2007**, *32*, 2453–2455.

(9) Shaikh, P. A.; Shi, D.; Retamal, J. R. D.; Sheikh, A. D.; Haque, M. A.; Kang, C. F.; He, J. H.; Bakr, O. M.; Wu, T. Schottky Junctions on Perovskite Single Crystals:

Light-Modulated Dielectric Constant and Self-Biased Photodetection. *J. Mater. Chem. C* **2016**, *4*, 8304–8312.

(10) Liu, S.; Zheng, F.; Koocher, N. Z.; Takenaka, H.; Wang, F.; Rappe, A. M. Ferroelectric Domain Wall Induced Band Gap Reduction and Charge Separation in Organometal Halide Perovskites. *J. Phys. Chem. Lett.* **2015**, *6*, 693–699.

(11) Kutes, Y.; Ye, L.; Zhou, Y.; Pang, S.; Huey, B. D.; Padture, N. P. Direct Observation of Ferroelectric Domains in Solution-Processed $CH_3NH_3PbI_3$ Perovskite Thin Films. *J. Phys. Chem. Lett.* **2014**, *5*, 3335–3339.

(12) Swainson, I. P.; Stock, C.; Parker, S. F.; Van Eijck, L.; Russina, M.; Taylor, J. W. From Soft Harmonic Phonons to Fast Relaxational Dynamics in $CH_3NH_3PbBr_3$. *Phys. Rev. B* **2015**, *92*, 100303.

(13) Frost, J. M.; Butler, K. T.; Brivio, F.; Hendon, C. H.; Van Schilfgaarde, M.; Walsh, A. Atomistic Origins of High-Performance in Hybrid Halide Perovskite Solar Cells. *Nano Lett.* **2014**, *14*, 2584–2590.

(14) Gao, Y.; Wang, S.; Huang, C.; Yi, N.; Wang, K.; Xiao, S.; Song, Q. Room Temperature Three-Photon Pumped $CH_3NH_3PbBr_3$ Perovskite Microlasers. *Sci. Rep.* **2017**, *7*, 45391.

(15) Johnson, J. C.; Li, Z.; Ndione, P. F.; Zhu, K. Third-Order Nonlinear Optical Properties of Methylammonium Lead Halide Perovskite Films. *J. Mater. Chem. C* **2016**, *4*, 4847–4852.

(16) Walters, G.; Sutherland, B. R.; Hoogland, S.; Shi, D.; Comin, R.; Sellan, D. P.; Bakr, O. M.; Sargent, E. H. Two-Photon Absorption in Organometallic Bromide Perovskites. *ACS Nano* **2015**, *9*, 9340–9346.

(17) Lee, M. M.; Teuscher, J.; Miyasaka, T.; Murakami, T. N.; Snaith, H. J. Efficient Hybrid Solar Cells Based on Meso-Superstructured Organometal Halide Perovskites. *Science* **2012**, *338*, 643–647.

(18) Park, N. G. Organometal Perovskite Light Absorbers toward a 20% Efficiency Low-Cost Solid-State Mesoscopic Solar Cell. *J. Phys. Chem. Lett.* **2013**, *4*, 2423–2429.

(19) Snaith, H. J. Perovskites: The Emergence of a New Era for Low-Cost, High-Efficiency Solar Cells. *J. Phys. Chem. Lett.* **2013**, *4*, 3623–3630.

(20) Zhou, H.; Chen, Q.; Li, G.; Luo, S.; Song, T. B.; Duan, H. S.; Hong, Z.; You, J.; Liu, Y.; Yang, Y. Interface Engineering of Highly Efficient Perovskite Solar Cells. *Science* **2014**, *345*, 542–546.

(21) Tan, Z. K.; Moghaddam, R. S.; Lai, M. L.; Docampo, P.; Higler, R.; Deschler, F.; Price, M.; Sadhanala, A.; Pazos, L. M.; Credgington, D.; *et al.* Bright Light-Emitting Diodes Based on Organometal Halide Perovskite. *Nat. Nanotechnol.* **2014**, *9*, 1–6.

(22) Gil-Escrig, L. N.; Longo, G.; Pertegá, A.; Roldá N-Carmona, C.; Soriano, A.; Sessolo, M.; Bolink, H. J. Efficient Photovoltaic and Electroluminescent Perovskite Devices. *Chem. Commun. Chem. Commun* **2015**, *51*, 569–571.

(23) Dou, L.; Yang, Y. M.; You, J.; Hong, Z.; Chang, W. H.; Li, G.; Yang, Y. Solution-Processed Hybrid Perovskite Photodetectors with High Detectivity. *Nat. Commun.* **2014**, *5*, 5404.

(24) Zhu, H.; Fu, Y.; Meng, F.; Wu, X.; Gong, Z.; Ding, Q.; Gustafsson, M. V; Trinh, M. T.; Jin, S.; Zhu, X. Y. Lead Halide Perovskite Nanowire Lasers with Low Lasing Thresholds and High Quality Factors. *Nat. Mater.* **2015**, *14*, 636–642.

(25) Lv, F.; Gao, C.; Zhou, H. A.; Zhang, P.; Mi, K.; Liu, X. Nonvolatile Bipolar Resistive

Switching Behavior in the Perovskite-like $(CH_3NH_3)_2FeCl_4$. *ACS Appl. Mater. Interfaces* **2016**, *8*, 18985–18990.

(26) Wei, T. C.; Wang, H. P.; Liu, H. J.; Tsai, D. S.; Ke, J. J.; Wu, C. L.; Yin, Y. P.; Zhan, Q.; Lin, G. R.; Chu, Y. H.; *et al.* Photostriction of Strontium Ruthenate. *Nat. Commun.* **2017**, *8*, 15018.

(27) Zhou, Y.; You, L.; Wang, S.; Ku, Z.; Fan, H.; Schmidt, D.; Rusydi, A.; Chang, L.; Wang, L.; Ren, P.; *et al.* Giant Photostriction in Organic–inorganic Lead Halide Perovskites. *Nat. Commun.* **2016**, *7*, 11193.

(28) Shi, D.; Adinolfi, V.; Comin, R.; Yuan, M.; Alarousu, E.; Buin, A.; Chen, Y.; Hoogland, S.; Rothenberger, A.; Katsiev, K.; *et al.* Low Trap-State Density and Long Carrier Diffusion in Organolead Trihalide Perovskite Single Crystals. *Science* **2015**, *347*, 519–522.

(29) Cai, B.; Xing, Y.; Yang, Z.; Zhang, W.-H.; Qiu, J. High Performance Hybrid Solar Cells Sensitized by Organolead Halide Perovskites. *Energy Environ. Sci.* **2013**, *6*, 1480.

(30) Liu, Y.; Yang, Z.; Cui, D.; Ren, X.; Sun, J.; Liu, X.; Zhang, J.; Wei, Q.; Fan, H.; Yu, F.; *et al.* Two-Inch-Sized Perovskite $CH_3NH_3PbX_3$ (X = Cl, Br, I) Crystals: Growth and Characterization. *Adv. Mater.* **2015**, *27*, 5176–5183.

(31) Watanabe, Y.; Sota, T.; Suzuki, K.; Iyi, N.; Kitamura, K.; Kimura, S. Defect Structures in $LiNbO_3$. *J. Phys. Condens. Matter* **1995**, *7*, 3627–3635.

(32) Eimerl, D.; Davis, L.; Velsko, S.; Graham, E. K.; Zalkin, A. Optical, Mechanical, and Thermal Properties of Barium Borate. *J. Appl. Phys.* **1987**, *62*, 1968–1983.

(33) Juarez-Perez, E. J.; Hawash, Z.; R. Raga, S.; Ono, L. K.; Qi, Y. Thermal Degradation

of $CH_3NH_3PbI_3$ Perovskite into NH_3 and CH_3I Gases Observed by Coupled Thermogravimetry - Mass Spectrometry Analysis. *Energy Environ. Sci.* **2016**, 9, 3406-3410.

(34) Taheri, B.; Liu, H.; Jassemnejad, B.; Appling, D.; Powell, R. C.; Song, J. J. Intensity Scan and Two Photon Absorption and Nonlinear Refraction of C 60 in Toluene. *Appl. Phys. Lett.* **1995**, *68*, 1317.

(35) Zheng, X.; Chen, B.; Yang, M.; Wu, C.; Orler, B.; Moore, R. B.; Zhu, K.; Priya, S. The Controlling Mechanism for Potential Loss in $CH_3NH_3PbBr_3$ Hybrid Solar Cells. *ACS Energy Lett.* **2016**, *1*, 424–430.

(36) Chen, H.; Zheng, X.; Li, Q.; Yang, Y.; Xiao, S.; Hu, C.; Bai, Y.; Zhang, T.; Wong, K. S.; Yang, S. An Amorphous Precursor Route to the Conformable Oriented Crystallization of $CH_3NH_3PbBr_3$ in Mesoporous Scaffolds: Toward Efficient and Thermally Stable Carbon-Based Perovskite Solar Cells. *J. Mater. Chem. A* **2016**, *4*, 12897–12912.

(37) Benninger, R. K. P.; Piston, D. W. Two-Photon Excitation Microscopy for the Study of Living Cells and Tissues. *Curr. Protoc. Cell Biol.* **2013**, *Chapter 4*, Unit 4.11.1-24.

(38) Fang, X.; Zhang, K.; Li, Y.; Yao, L.; Zhang, Y.; Wang, Y.; Zhai, W.; Tao, L.; Du, H.; Ran, G. Effect of Excess $PbBr_2$ on Photoluminescence Spectra of $CH_3NH_3PbBr_3$ Perovskite Particles at Room Temperature. *Appl. Phys. Lett.* **2016**, *108*, 071109.

(39) Ibrahim Dar, M.; Abdi-Jalebi, M.; Arora, N.; Moehl, T.; Grätzel, M.; Nazeeruddin, M. K. Understanding the Impact of Bromide on the Photovoltaic Performance of CH3NH3PbI3 Solar Cells. *Adv. Mater.* **2015**, *27*, 7221–7228.

(40) Boyd, R. W. Nonlinear Optics. *Acad. Press* **2008**, 613.

(41) Seyler, K. L.; Schaibley, J. R.; Gong, P.; Rivera, P.; Jones, A. M.; Wu, S.; Yan, J.; Mandrus, D. G.; Yao, W.; Xu, X. Electrical Control of Second-Harmonic Generation in a WSe_2 Monolayer Transistor. *Nat Nano* **2015**, *10*, 407–411.

(42) Deckoff-Jones, S.; Zhang, J. J.; Petoukhoff, C. E.; Man, M. K. L.; Lei, S. D.; Vajtai, R.; Ajayan, P. M.; Talbayev, D.; Madeo, J.; Dani, K. M. Observing the Interplay between Surface and Bulk Optical Nonlinearities in Thin van Der Waals Crystals. *Sci. Rep.* **2016**, *6*, 7.

(43) Chen, T.; Foley, B. J.; Ipek, B.; Tyagi, M.; Copley, J. R. D.; Brown, C. M.; Choi, J. J.; Lee, S. H. Rotational Dynamics of Organic Cations in $CH_3NH_3PbI_3$ Perovskite. *Phys. Chem. Chem. Phys.* **2015**, *17*, 31278-31286.

(44) Lee, J. H.; Lee, J. H.; Kong, E. H.; Jang, H. M. The Nature of Hydrogen-Bonding Interaction in the Prototypic Hybrid Halide Perovskite, Tetragonal $CH_3NH_3PbI_3$. *Sci. Rep.* **2016**, *6*, 21687.

(45) Sorianello, V.; Colace, L.; Nardone, M.; Assanto, G. Thermally Evaporated Single-Crystal Germanium on Silicon. *Thin Solid Films* **2011**, *519*, 8037–8040.

(46) Juodawlkis, P. W.; Plant, J. J.; Donnelly, J. P.; Motamedi, A.; Ippen, E. P. Continuous-Wave Two-Photon Absorption in a Watt-Class Semiconductor Optical Amplifier. *Opt. Express* **2008**, *16*, 12387.

(47) Duchesne, D.; Rutkowska, K. a; Volatier, M.; Légaré, F.; Delprat, S.; Chaker, M.; Modotto, D.; Locatelli, a; De Angelis, C.; Sorel, M.; *et al.* Second Harmonic Generation in AlGaAs Photonic Wires Using Low Power Continuous Wave Light. *Opt. Express* **2011**, *19*, 12408–12417.

(48) Sheik-Bahae, M.; Said, A. A.; Wei, T.-H.; Hagan, D. J.; Van Stryland, E. W. Sensitive Measurement of Optical Nonlinearities Using a Single Beam. *IEEE J. Quantum Electron.* **1990**, *26*, 760–769.

(49) Zhang, Y.-D.; Zhao, Z.-Y.; Yao, C.-B.; Yang, L.; Li, J.; Yuan, P. The Nonlinear Absorption and Optical Limiting in Phenoxy-Phthalocyanines Liquid in Nano- and Femto-Second Regime: Experimental Studies. *Opt. Laser Technol.* **2014**, *58*, 207–214.

(50) Guang S. He, Qingdong Zheng, Ken-Tye Yong, Aleksandr I. Ryasnyanskiy, and P. N. P. Two-Photon Absorption Based Optical Limiting and Stabilization by Using a CdTe Quantum Dot Solution Excited at Optical Communication Wavelength of ∼1300nm. *Appl. Phys. Lett.* **2007**, *90*, 181108.

(51) Allakhverdiev, K. R. Two-Photon Absorption in Layered $TlGaSe_2$, $TlInS_2$, $TlGaS_2$ and GaSe Crystals. *Solid State Commun.* **1999**, *111*, 253–257.

(52) Beyer, O.; Maxein, D.; Buse, K.; Sturman, B.; Hsieh, H. T.; Psaltis, D. Investigation of Nonlinear Absorption Processes with Femtosecond Light Pulses in Lithium Niobate Crystals. *Phys. Rev. E - Stat. Nonlinear, Soft Matter Phys.* **2005**, *71*, 056603.

(53) Carson, A.; Anderson, M. E. Two-Photon Absorption and Blue-Light-Induced Red Absorption in LiTaO3 Waveguides. *JOSA B* **2006**, *23*, 1129–1136.

(54) Maslov, V. A.; Mikhailov, V. A.; Shaunin, O. P.; Shcherbakov, I. A. Nonlinear Absorption in KTP Crystals. *Quantum Electron.* **1997**, *27*, 356–359.

(55) Wang, D.; Li, T.; Wang, S.; Wang, J.; Shen, C.; Ding, J.; Li, W.; Huang, P.; Lu, C. Characteristics of Nonlinear Optical Absorption and Refraction for KDP and DKDP Crystals. *Opt. Mater. Express* **2017**, *7*, 533–541.

(56) Yamada, H.; Shirane, M.; Chu, T.; Yokoyama, H.; Ishlda, S.; Arakawa, Y. Nonlinear-Optic Silicon-Nanowire Waveguides. *Japanese J. Appl. Physics, Part 1 Regul. Pap. Short Notes Rev. Pap.* **2005**, *44*, 6541–6545.

(57) Lin, Q.; Zhang, J.; Piredda, G.; Boyd, R. W.; Fauchet, P. M.; Agrawal, G. P. Dispersion of Silicon Nonlinearities in the near Infrared Region. *Appl. Phys. Lett.* **2007**, *91*, 021111.

(58) Tong, X. C. *Advanced Materials for Integrated Optical Waveguides*; Springer Series in Advanced Microelectronics; Springer International Publishing, 2013.

(59) He, G. S.; Tan, L.-S.; Zheng, Q.; Prasad, P. N. Multiphoton Absorbing Materials: Molecular Designs, Characterizations, and Applications. *Chem. Rev.* **2008**, *108*, 1245–1330.

(60) Tutt, L. W.; Boggess, T. F. A Review of Optical Limiting Mechanisms and Devices Using Organics, Fullerenes, Semiconductors and Other Materials. *Prog. quantum Electron.* **1993**, *17*, 299–338.

(61) He, G. S.; Gvishi, R.; Prasad, P. N.; Reinhardt, B. A. Two-Photon Absorption Based Optical Limiting and Stabilization in Organic Molecule-Doped Solid Materials. *Opt. Commun.* **1995**, *117*, 133–136.

(62) He, G. S.; Lin, T. C.; Prasad, P. N.; Cho, C. C.; Yu, L. J. Optical Power Limiting and Stabilization Using a Two-Photon Absorbing Neat Liquid Crystal in Isotropic Phase. *Appl. Phys. Lett.* **2003**, *82*, 4717–4719.

(63) He, G. S.; Yuan, L.; Cheng, N.; Bhawalkar, J. D.; Prasad, P. N.; Brott, L. L.; Clarson, S. J.; Reinhardt, B. A. Nonlinear Optical Properties of a New Chromophore. *J. Opt. Soc. Am. B* **1997**, *14*, 1079–1087.

(64) Tull, J. X.; Dugan, M. A.; Warren, W. S. High-Resolution, Ultrafast Laser Pulse Shaping and Its Applications. *Adv. Magn. Opt. Reson.* **1997**, *20*, 1–II.

(65) He, G. S.; Swiatkiewicz, J.; Jiang, Y.; Prasad, P. N.; Reinhardt, B. A.; Tan, L.-S.; Kannan, R. Two-Photon Excitation and Optical Spatial-Profile Reshaping via a Nonlinear Absorbing Medium. *J. Phys. Chem. A* **2000**, *104*, 4805–4810.

(66) He, G. S.; Yuan, L.; Bhawalkar, J. D.; Prasad, P. N. Optical Limiting, Pulse Reshaping, and Stabilization with a Nonlinear Absorptive Fiber System. *Appl. Opt.* **1997**, *36*, 3387–3392.

(67) Perry, J. W.; Mansour, K.; Lee, I. Y. S.; Wu, X. L.; Bedworth, P. V.; Chen, C. T.; Ng, D.; Marder, S. R.; Miles, P.; Wada, T.; *et al.* Organic Optical Limiter with a Strong Nonlinear Absorptive Response. *Science* **1996**, *273*, 1533–1536.

(68) Xu, Y.; Liu, Z.; Zhang, X.; Wang, Y.; Tian, J.; Huang, Y.; Ma, Y.; Zhang, X.; Chen, Y. A Graphene Hybrid Material Covalently Functionalized with Porphyrin: Synthesis and Optical Limiting Property. *Adv. Mater.* **2009**, *21*, 1275–1279.

(69) Heisterkamp, A.; Ripken, T.; Mamom, T.; Drommer, W.; Welling, H.; Ertmer, W.; Lubatschowski, H. Nonlinear Side Effects of Fs Pulses inside Corneal Tissue during Photodisruption. *Appl. Phys. B Lasers Opt.* **2002**, *74*, 419–425.

(70) Shi, D.; Adinolfi, V.; Comin, R.; Yuan, M.; Alarousu, E.; Buin, A.; Chen, Y.; Hoogland, S.; Rothenberger, A.; Katsiev, K.; *et al.* Low Trap-State Density and Long Carrier Diffusion in Organolead Trihalide Perovskite Single Crystals. *Science* **2015**, *347*, 519–522.